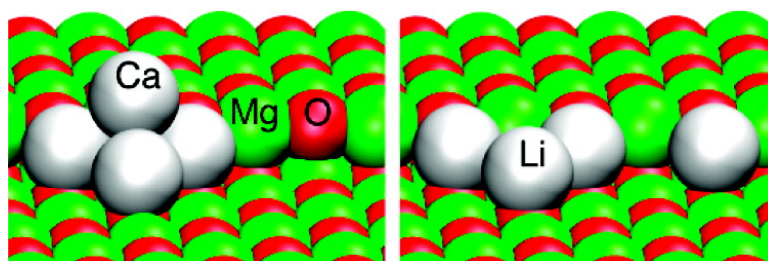**Article**

Defect Sites and Their Distributions on MgO(100) by Li and Ca Adsorption Calorimetry

Jason A. Farmer, Charles T. Campbell, Lijun Xu, and Graeme Henkelman

More About This Article

Additional resources and features associated with this article are available within the HTML version:

- Supporting Information
- Access to high resolution figures
- Links to articles and content related to this article
- Copyright permission to reproduce figures and/or text from this article

View the Full Text HTML

Defect Sites and Their Distributions on MgO(100) by Li and Ca Adsorption Calorimetry

Jason A. Farmer,[†] Charles T. Campbell,*,[†] Lijun Xu,[‡] and Graeme Henkelman*,[‡]

Department of Chemistry, University of Washington, Seattle, Washington 98195-1700, and Department of Chemistry and Biochemistry, University of Texas at Austin, Austin, Texas 78712-0165

Received November 16, 2008; E-mail: campbell@chem.washington.edu; henkelman@mail.utexas.edu

Abstract: Chemical bonding to oxide surfaces is often dominated by surface defects, but their nature remains elusive. Calorimetric measurements of Ca and Li adsorption energies on MgO(100) and ion-damaged MgO(100), when combined with density functional theory (DFT) calculations and kinetic modeling, are shown to be a powerful way to assess the nature of the defect sites on oxide surfaces and their lateral distributions. While ion sputtering causes a strong increase in the initial adsorption energy for Li on MgO(100) at 300 K, the initial adsorption energy for Ca is independent of the extent of sputtering. This result and the measured coverage dependence of the adsorption energies of Ca and Li on MgO(100) surfaces with ~5, 12, and 25% defects were simulated with a kinetic model based on DFT input regarding site binding energies and adatom migration barriers. Reproducing the experimental results required models with distinct probability distributions of local defect concentrations for the differing extents of ion damage. A key difference between Li and Ca revealed by DFT and necessary to reproduce their differing adsorption energy versus ion damage measurements is the much greater tendency for a diffusing Li adatom to remain locked in place once it reaches a terrace site neighboring an occupied step or kink site, thus nucleating a 2D island on a terrace. In contrast, Ca adatoms thermally diffuse from such sites quickly, to seek out the remaining defect sites. The model also reproduces the measured Li and Ca film morphology seen by ion scattering spectroscopy.

Introduction

The chemistry occurring on oxide surfaces is important in a wide variety of applications including catalytic materials, photovoltaic devices, photocatalysts, microelectronics fabrication, and ceramic-containing composite materials. Chemical bonding to oxide surfaces is often dominated by surface defect sites. For example, organic molecules preferentially bind and dissociate at oxide defects, and metal nanoparticles in oxide-supported later transition metal catalysts usually nucleate at surface defects on the oxide. Thus, the nature and concentration of defect sites are very important in the surface chemistry of oxides, yet their experimental elucidation generally remains only qualitative. Here we show that calorimetric measurements of Ca and Li adsorption energies on MgO(100), and ion-damaged MgO(100), at 300 K, when combined with DFT calculations and kinetic modeling, offer a powerful way to assess the nature of the defect sites on oxide surfaces, their concentrations, and even the probability distributions of local defect concentration across the surface.

Lithium-promoted magnesium oxide is an important catalyst for selective methane and small alkane oxidation.[1-3] Adsorbed Li on MgO(100) is also one of the very few metal adsorbates on any single-crystal oxide surface that has been characterized

by electron spin resonance.[4,5] It has also been the subject of much other experimental and theoretical study.[3-8] Studies of other alkali metals on MgO(100) found that surface defect sites act as nucleation centers for 3D particle growth.[9,10] Both Li and Ca are common promoters present on oxide surfaces in industrial catalysts.

We reported elsewhere single-crystal adsorption microcalorimetry measurements, supported with AES, ISS, and work function measurements, of Ca adsorption on MgO(100) thin films (4 nm thick) grown on Mo(100) and on ion-sputtered MgO(100) surfaces.[11] Here we present similar results for Li adsorption on MgO(100) and ion-damaged MgO(100), comparing and contrasting them to those results for Ca. A more detailed presentation of these Li/MgO results, especially the structural and electronic aspects, will be presented elsewhere.[12] These data

---

† University of Washington.
‡ University of Texas at Austin.

(1) Lunsford, J. H. *Angew. Chem., Int. Ed. Engl.* **1995**, *34*, 970–980.
(2) Kuo, Y.; Behrendt, F.; Lerch, M. *Z. Phys. Chem.* **2007**, *221*, 1017–1037.
(3) Scanlon, D. O.; Walsh, A.; Morgan, B. J.; Nolan, M.; Fearon, J.; Watson, G. W. *J. Phys. Chem. C* **2007**, *111*, 7971–7979.
(4) Finazzi, E.; Di Valentin, C.; Pacchioni, G.; Chiesa, M.; Giamello, E.; Gao, H. J.; Lian, J. C.; Risse, T.; Freund, H. J. *Chem.−Eur. J.* **2008**, *14* (14), 4404–4414.
(5) Lian, J. C.; Finazzi, E.; Di Valentin, C.; Risse, T.; Gao, H. J.; Pacchioni, G.; Freund, H. J. *Chem. Phys. Lett.* **2008**, *450*, 308–311.
(6) Snyder, J. A.; Jaffe, J. E.; Gutowski, M.; Lin, Z. J.; Hess, A. C. *J. Chem. Phys.* **2000**, *112*, 3014–3022.
(7) Giamello, E.; Murphy, D.; Ravera, L.; Coluccia, S.; Zecchina, A. *J. Chem. Soc., Faraday Trans.* **1994**, *90* (20), 3167–3174.
(8) Brazzelli, S.; Di Valentin, C.; Pacchioni, G.; Giamello, E.; Chiesa, M. *J. Phys. Chem. B* **2003**, *107*, 8498–8506.
(9) Kendelewicz, T.; Liu, P.; Brown, G. E.; Nelson, E. J.; Pianetta, P. *Surf. Sci.* **1996**, *352−354*, 451–456.
(10) Brause, M.; Ochs, D.; Gunster, J.; Mayer, T.; Braun, B.; Puchin, V.; Maus-Friedrichs, W.; Kempter, V. *Surf. Sci.* **1997**, *383*, 216–225.
(11) Zhu, J. F.; Farmer, J. A.; Ruzycki, N.; Xu, L.; Campbell, C. T.; Henkelman, G. *J. Am. Chem. Soc.* **2008**, *130*, 2314–2322.
(12) Farmer, J. A.; Ruzycki, N.; Campbell, C. T. Manuscript in preparation.
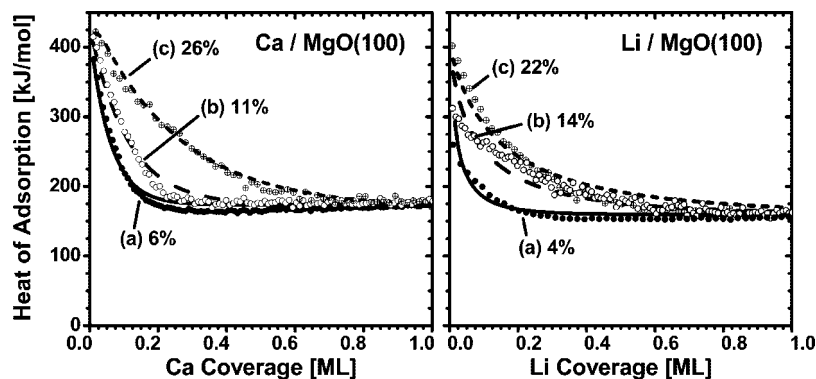
Figure 1. Heat of adsorption of Ca (left panel) and Li (right panel) versus coverage at 300 K for adsorption on (a) pristine MgO(100) and (b)−(c) MgO(100) irradiated with increasing Ar$^+$ ion doses (10^{14}−10^{16} ions/cm^2) to create more defects. Each data point is due to a pulse of 0.006−0.015 ML of metal (pulsed at 1/2 Hz) and is the average of three or four identical experimental runs, except curves (b) and (c) for Li, which were single runs. The curves through the data represent theoretical simulations of a model based on DFT energetics described in the text. Each curve is labeled with the percentage of total MgO sites which were defect sites, according to this model.

are analyzed here based on DFT calculations of the appropriate binding energies and metal adatom migration energies, which we have published previously for Ca/MgO(100)[11,13] and which will be described in more detail for Li/MgO(100) in a forthcoming publication.[14]

Materials and Methods

Experimental Methods. The microcalorimetry experiment and apparatus have been described in detail previously.[15] The calorimeter was housed in an ultrahigh vacuum chamber, with a base pressure of ∼2 × 10^{-10} mbar (rising to ∼1 × 10^{-9} mbar due to H$_2$ outgassing during Li deposition). It was equipped with LEED, AES, and He$^+$ ion-scattering spectroscopy, a quadrupole mass spectrometer (QMS), and a quartz crystal microbalance (QCM). The details of all the measurement methods and the preparation and annealing of the 4-nm-thick MgO(100) thin film are the same as described in our study of Ca on MgO(100).[11] A more detailed description of a few minor experimental differences specific to this Li/MgO(100) system will be presented elsewhere.[12]

Theoretical Methods. The energetics of Ca and Li binding to MgO(100) were calculated with density functional theory (DFT). The details of these calculations are presented elsewhere.[11,13,14] In short, the MgO(100) slab is represented by 18−36 atoms per layer and 2−3 layers with the bottom layer(s) frozen. The Brillouin zone is sampled at the Gamma point and using a 2 × 2 × 1 Monkhorst Pack mesh to check for convergence of binding energies. A plane wave basis set with a cutoff energy of 274 eV was used to represent the wave functions, and the PW91 functional to describe electronic correlation. The climbing-image nudged elastic band method was used to determine the geometry and energy of transition states between stable minima.[16] All geometries were optimized until the force on each atom dropped below 0.002 eV/Å.

Results and Discussion

Experimental Heats of Adsorption versus Coverage and Defect Density. The left panel in Figure 1 shows the differential heat of adsorption of Ca on a freshly prepared MgO(100) thin film (pristine MgO(100)) as a function of Ca coverage, and on MgO(100) thin films after adding two different concentrations of extra surface defects by ion sputtering. The right panel shows the same type data, but for Li adsorption. One monolayer (ML)

is defined for both Ca and Li as 1.12 × 10^{15} atoms/cm^2, which is the MgO(100) unit cell density. The surface defects were added by lightly sputtering the pristine MgO(100) surface at 300 K with Ar$^+$ ions (1000 eV). Experimental studies of Ar$^+$ bombardment of MgO(100) have shown that the surface stoichiometry does not change significantly during bombardment[17−19] and that the dominant structural unit removed from the oxide surface was clusters of MgO, leaving divacancies on the surface.[20] Other studies done using EELS on sputter-damaged MgO(100) films showed that band-gap states produced by sputtering could be "healed" by oxygen dosing but did not rule out other types of defect formation from sputtering.[21] The data in Figure 1 were acquired with the surface at 300 K but with Ca or Li gas from a hot source. The heats here have been corrected by the difference in source temperature (and atomic beam directionality) as described elsewhere,[15] so that they reflect the standard enthalpy of adsorption at 300 K. The curves through the data points represent a theoretical simulation described below. The defect concentration labeling each curve was determined as a fitting parameter from those simulations. It is proportional to the coverage-integrated heat of adsorption after subtracting the high-coverage limit (equal to the bulk heat of sublimation in each case).

These Ca data have been presented and analyzed previously,[11] and we now summarize those results. On pristine MgO(100), AES and ISS measurements showed that Ca grows mainly as 3D particles with a density of ∼1 × 10^{12} islands/cm^2. Ca adsorbs initially at defect sites with a very high heat of adsorption (∼410 kJ/mol). DFT calculations attribute this high initial heat to Ca binding to kink sites (347 kJ/mol), step sites (203 kJ/mol), and lower concentrations of stronger binding defect sites. The heat of adsorption decreases rapidly with coverage, reaching a minimum of 162 kJ/mol at ∼0.3 ML, where Ca is mainly adding to small 3D Ca clusters. This decrease in heat was attributed to the decreasing probability of finding defect sites as they become saturated and an increasing probability of populating sites on

(13) Xu, L.; Henkelman, G. *Phys. Rev. B* **2008**, *77*, 205404.

(14) Xu, L.; Henkelman, G. Manuscript in preparation.

(15) Stuckless, J. T.; Frei, N. A.; Campbell, C. T. *Rev. Sci. Instrum.* **1998**, *69*, 2427–2438.

(16) Henkelman, G.; Jonsson, H. *J. Chem. Phys.* **2000**, *113* (22), 9978–9985.

(17) Smentkowski, V. S. *Prog. Surf. Sci.* **2000**, *64*, 1–58.

(18) Bertoti, I.; Kelly, R.; Mohai, M.; Toth, A. *Surf. Interface Anal.* **1992**, *19*, 291–297.

(19) Marletta, G.; Iacona, F.; Kelly, R. *Nucl. Instrum. Methods Phys. Res., Sect. B* **1992**, *65*, 97–101.

(20) Malherbe, J. B.; Hofmann, S.; Sanz, J. M. *Appl. Surf. Sci.* **1986**, *27*, 355–365.

(21) Peterka, D.; Tegenkamp, C.; Schroder, K. M.; Ernst, W.; Pfnur, H. *Surf. Sci.* **1999**, *431* (1−3), 146–155.

Table 1. DFT Energies for Metal Adsorption E_{ads} (kJ/mol) at Various Sites on MgO(100) and Diffusion Barrier E_{act} (kJ/mol) for Any Atom Leaving the Site to Get to the Most Stable Neighboring Site on MgO[a]

	Ca		Li	
site[b]/energy	E_{ads} (kJ/mol)	E_{act} (kJ/mol)	E_{ads} (kJ/mol)	E_{act} (kJ/mol)
terrace	82	43.4	78	45.3
step[c]	205	135	161	122
kink[c]	376	(294.45)	343	(310)
F-center	35	tiny	55	(22.3)
F$^+$-center	73	(34.4)	132	(99.3)
NN to monomer on terrace	88	(49.4)	134	(100)
NN to monomer at step[d]	80	(<40)	141	20
NN to dimer along step[d]	99	31	134	(100)
NN to 2D island[e]	100	(52.6) up-step = 13	116	(95.6) up-step = 26
c(2 × 2) half-monolayer[f]	123	–	104	–
monolayer[f]	unstable	–	141	–
bulk solid[f]	181	–	156	–

[a] "NN" refers to nearest-neighbor sites. Numbers in parentheses are estimated as the binding energy difference plus the terrace−monomer diffusion barrier. From refs 11, 13, and 14. [b] Except at oxygen vacancies, all stable sites are above (atop) oxygen anions. Step sites are at the lower edge of straight, nonpolar step edges composed of alternating Mg and O ions. See ref 13 for drawings of all sites. [c] The barriers from steps and kinks are the barriers to leave that site to go to a neighboring terrace site, but since this is the lowest-energy pathway to reach a neighboring step site (which is a two-step process), these also equal the barrier to go to the nearest step site. [d] The "NN to monomer at step" and "NN to dimer along step" sites are the most stable terrace sites adjacent to a monomer at or dimer along a step edge. The barrier for the "NN to monomer at step" is small because this terrace adatom is moving to the much more stable step site adjacent to the step monomer. [e] This 2D island is a square, planar tetramer, so this NN makes it a 2D pentamer. The second barrier is that for its NN to up-step to layer two. [f] The bottom three rows refer to the adsorption energy to make that complete, infinite structure starting from clean MgO(100) and metal gas atoms. "Monolayer" refers to a flat (1 × 1) monolayer for Li, but for Ca that structure is not possible (due to the large size of Ca) and it puckers even at 0 K into a stable bilayer of c(2 × 2) overlayers with adsorption energy 155 kJ/mol. Small 2D Ca islands are, however, stable in a stretched (1 × 1) geometry, so that is the geometry used here for the "NN to 2D island" entry for both Li and Ca.

Ca clusters, which nucleate at defects. These include both terrace sites at the edges of clusters and sites on top of clusters. These results require Ca to be more weakly bound to MgO(100) terraces as monomers or as 2D clusters than to 3D Ca particles and to diffuse rapidly at room temperature across MgO(100) terraces, which was verified by DFT. Above 0.3 ML, the heat increases to the bulk Ca heat of sublimation (178 kJ/mol) by ~1.2 ML, with this rise attributed to the increase in Ca stability within clusters as their size increases, a particle size effect which has been observed for other metals.[22] Adding more defects by ion bombardment does not change the initial heat of adsorption significantly but causes the heat to decrease more slowly with Ca coverage, which was attributed to creation of the same types of defects in approximately the same site concentration ratio as on the pristine surface.

The Li data in Figure 1 have not appeared previously. Our ISS and AES measurements showed that Li is adsorbing mainly in the first layer below 0.25 ML but starts adding to the second layer after that, with mainly 3D growth above 0.6 ML (see below). On pristine MgO(100), the heat of Li adsorption starts at 260 kJ/mol but drops rapidly with coverage to reach a minimum of 153 kJ/mol by 0.4 ML. Thereafter, the heat increased slightly to the bulk heat of sublimation of Li (159 kJ/mol[23]) by ~1.5 ML. Again, we will attribute the initially high heat of adsorption at low coverage and its decrease to a minimum to Li adatoms populating intrinsic defect sites and their preferential saturation with increasing coverage. This is also consistent with DFT calculations presented below. The small, asymptotic rise from the minimum to the heat of sublimation is again attributed to the formation of larger Li particles on the surface and the lower stability of Li in smaller clusters. Also shown in Figure 1 is the effect of added defects

from sputtering with Ar$^+$ ions for a low dose (1 × 10^{14} ions/cm^2) and a high dose (7.5 × 10^{14} ions/cm^2). As with Ca, addition of surface defects causes the initial heat of Li adsorption to decrease more slowly with coverage, but unlike Ca, this increases the initial heat of Li adsorption. The increase is large: ~50 and ~140 kJ/mol above the pristine surface value for the low- and high-ion doses, respectively.

Simulation of Adsorption Energies Using DFT-Calculated Adatom Energetics. Next, we present a simple model based on energetics calculated with DFT to semiquantitatively fit these decreases in adsorption energy with coverage for Ca and Li and their dependences on defect density. These fits are shown as the curves through the data in Figure 1. An important aspect of this model is that it reproduces semiquantitatively the dependence of the initial heat of adsorption for Li on defect density and its lack of dependence for Ca. This required a detailed description of the defect concentration and its variation across the surface, which provides unique insight into defect distributions on this much-studied oxide surface.

For Ca, the independence of its initial heat of adsorption on the extent of sputter damage in Figure 1 was attributed previously to Ca adsorbing in defect sites *only* for all coverages below 0.02 ML, with roughly the same ratios of concentrations of different defect types independent of total defect density.[11] This was supported by our DFT slab calculations' estimates of Ca adatom energetics (see Table 1). These show that the adsorption energies at kinks, steps, and Mg vacancies are large and that the activation barriers for Ca adatom migration are very low for Ca to diffuse from any type of site except from defects, but so high from most defects (kinks, Mg vacancies, steps, and even along steps) that migration would be prevented at 300 K. Thus, these defects would be populated irreversibly and in ratios proportional to their relative concentrations.

For Li, but unlike Ca, sputter damage increases the initial heat of adsorption in Figure 1. The energetics from our DFT slab calculations, summarized in Table 1 and presented in more detail elsewhere,[11,13,14] rule out many models that might explain

(22) Campbell, C. T.; Parker, S. C.; Starr, D. E. *Science* **2002**, *298* (5594), 811–814.
(23) Lide, D. R. *CRC Handbook of Chemistry and Physics (Internet Version)*, 88th ed.; CRC Press/Taylor and Francis: Boca Raton, FL, 2008.

this. For example, since Li (like Ca) cannot diffuse along step edges at 300 K, this cannot be attributed to kinks being preferentially populated relative to step sites initially. We will attribute this increase to the fact some Li atoms should not adsorb at defects in the first 0.02 ML pulse (according to DFT energetics), but that a greater fraction of them should adsorb at defect sites when the defect concentration is higher. In our model, this happens because, even in the first pulse of the atomic beam, some Li atoms get kinetically trapped in terrace adsorption sites (at the edges of preadsorbed Li clusters, which nucleated at defects). This prevents them from reaching the more stable defect adsorption sites. The Li adatom energetics in Table 1 naturally result in this behavior, as we explain next.

The DFT energy barriers for migration in Table 1 show that Li monomers diffuse rapidly across terraces at 300 K, but they get kinetically trapped at terrace sites at the edges of 2D Li clusters, which nucleate at step edges. This prevents them from reaching the stronger binding defect sites. These trap sites have a small adsorption energy for Li, near the heat of sublimation, and therefore they lower the average Li adsorption energy when their population is comparable to the defect site population. For Ca adatoms, this same migration barrier is 43 kJ/mol lower and quickly accessible at 300 K (jump time ~ 3500/s), and so these terrace sites at the edges of 2D Ca clusters do *not* trap the diffusing Ca. Also, Li adatoms at these trap sites at the edges of 2D islands are 20 kJ/mol more stable than Ca adatoms, relative to their respective terrace monomers. This difference aids in this effect but is not as important as the larger barrier difference between Li and Ca.

A numerical simulation of the model outlined above involving these trap sites, assuming equal *a priori* probabilities, is sufficient to semiquantitatively reproduce the heats of adsorption for Ca and Li versus coverage and defect concentration, again assuming that the ratio of concentrations of different defect types is independent of total defect density. The curves through the data in Figure 1 show the fits to the data with this model, which was evaluated at the experimental coverages. For each coverage value, it was assumed that all deposited atoms were able to diffuse rapidly across MgO terraces and irreversibly bind either to an existing cluster or to a defect, For simplicity, all defect sites were assumed to have a single adsorption energy (q_{defect} = 420 kJ/mol for Ca, 400 kJ/mol for Li), and all sites on top of clusters or in terrace sites at the edges of 2D or 3D clusters were assumed to have the same heat, equal to the bulk heat of sublimation (q_{sub} = 174 kJ/mol for Ca, 159 kJ/mol for Li[23]). For Ca, it was assumed that only defect sites are populated until all the defects are filled. After that, Ca grows exclusively on top of clusters or in terrace sites at the edges of 2D or 3D clusters (which nucleate from defects). For Li, once the defects become populated partially, it was assumed that a Li atom which lands on top of populated sites stays on top and that a Li atom which lands on free sites has a probability of finding an occupied defect equal to the fractional occupation of defect sites. If it finds an occupied defect, it was assumed to stop on a terrace site, binding to the Li atom(s) already at that defect (with a heat of adsorption equal to q_{sub}). This leads to first-order Langmuir-like kinetics for defect filling, such that the probability that an atom goes to a unoccupied defect decays as $\exp(-\theta/f_d)$, where θ is the metal coverage and f_d is the fraction of sites that are defects.

Fitting the data with this model further required recognizing that, on our MgO(100) surface, there is a distribution of sizes of defect-free terrace domains, which results in a distribution of local defect concentrations. Thus, the model above was treated
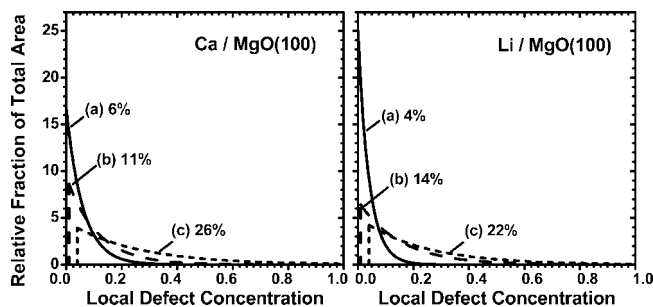

Figure 2. Probability distribution of local defect concentrations on (a) pristine MgO(100) and (b)−(c) MgO(100) irradiated with increasing Ar⁺ ion doses, as used to simulate the corresponding calorimetry data giving the heats of adsorption of Ca (left) and Li (right) versus coverage in Figure 1.

locally and then integrated across the surface. We define the local defect concentration, $f_{d,local}$, as the fraction of all local sites which are defects, where "local" is defined by the average area that could be probed by a diffusing adatom before it gets trapped at a defect. This fraction equals 4/*L* for large square or round terraces of width *L* (unit cell lengths) surrounded by steps. A variation in $f_{d,local}$ across the surface is clearly seen in STM images of similarly prepared MgO(100) thin films,[24] where the distances across terraces to the next defect vary widely. Thus, we assumed that there is a probability distribution of local defect concentrations, $W(f_{d,local})$, where $W(f_{d,local})\,df_{d,local}$ is the fraction of the total surface area with local defect concentrations between $f_{d,local}$ and $f_{d,local} + df_{d,local}$. As a simple mathematical representation of what we imagined to be the real physical situation, we assumed that this probability distribution decays exponentially with local defect concentration, but that, for the sputter-damaged surfaces, there are no defect-free terrace domains larger than a certain cutoff size (due to ion damage). This latter assumption is equivalent to setting $W(f_{d,local})$ to zero below some cutoff concentration ($f_{d,cr}$). This gives

$$W(f_{d,local}) = 0 \quad \text{when} \quad f_{d,local} < f_{d,cr} \tag{1}$$

$$W(f_{d,local}) = A\exp(-Cf_{d,local}) \quad \text{when} \quad f_{d,local} \geq f_{d,cr} \tag{2}$$

where $f_{d,cr} = 0$ for the unsputtered surface. The exponential decay constant (C) and this cutoff concentration were fitting parameters. The former essentially sets the average defect concentration and is easily chosen since it is proportional to the integrated area under the heat curve (after subtracting the heat of sublimation) within this model. The value of A is set by recognizing that the integral of $W(f_{d,local})$ equals unity, so it is not really a fitting parameter. Figure 2 shows the probability distributions of local defect concentrations which were required to fit the experimental heat curves of Figure 1 with this model.

The probability that a deposited atom reaches a defect site depends on the total deposited coverage θ and is given in this model for Ca by

$$P_{defect,Ca}(\theta) = \int_0^1 W(f_{d,local})\,\Theta(1 - \theta/f_{d,local})\,df_{d,local} \tag{3}$$

where Θ is the Heaviside step function. For Li, it is given by

$$P_{defect,Li}(\theta) = \int_0^1 W(f_{d,local})\exp(-\theta/f_{d,local})\,df_{d,local} \tag{4}$$

where this exponential factor is the probability that a Li atom finds an unoccupied defect in the region with a local defect

(24) Benedetti, S.; Benia, H. M.; Nilius, N.; Valeri, S.; Freund, H. J. *Chem. Phys. Lett.* **2006**, *430*, 330−335.

concentration $f_{d,local}$. The differential heat of adsorption is calculated from this probability for finding a defect

$$q_{ads}(\theta) = P_{defect,I}(\theta)q_{defect} + [1 - P_{defect,I}(\theta)]q_{sub} \qquad (5)$$

Figure 1 shows that this simple two-heat model reproduces all the salient features of the measured heats for both Li and Ca. In this model the heats are (a) the defect heat (a high heat) and (b) the average heat for atoms either in 3D clusters or on terraces in 2D clusters (a low heat). Table 1 shows that there are clearly many more heats than this, but they do group into these two categories. The kinetics of migration at 300 K implied by the barriers in Table 1 explain why all the strong binding defect types give a single heat. (Atoms cannot migrate from one defect to find a more stable defect.) Clearly a more accurate fit could be achieved by including more of the different adsorption energies of Table 1, but this is not necessary to understand the main differences between Li and Ca.

This addition of a distribution of local defect concentrations to our model makes a big difference in the way the heat decays with coverage for Ca, since without this it would appear as a step-function decrease from q_{defect} to q_{sub} once the defects are populated. Our earlier analysis of the coverage dependence for Ca[11] fit its exponential decay using the same type model we describe above for Li. (That is, it was assumed if a Ca on a terrace diffuses next to an occupied defect, it stops on that terrace site, binding to the Ca atom(s) already at that defect with a heat of adsorption equal to q_{sub}.) However, the DFT energetics of Table 1 prove that this would only happen for Li. A Ca adatom would <u>not</u> get trapped at such a site at 300 K! Thus, this more complex model was demanded.

Point defects on MgO(100) surfaces (O vacancies on terraces, Mg vacancies, and MgO divacancies) have been found to act as nucleation centers for metal particles.[25–27] The most common point defect is thought to be O vacancies (F, F^+, or F^{2+} sites), although previous studies have found that their concentration is tiny (less than a few percent of a ML) using our preparation technique,[28,29] and they mainly exist at step edges.[28,30] Table 1 also shows that Li-occupied F^+ sites would provide terrace trapping sites for diffusing Li atoms (adjacent to the Li in the vacancy site) that would kinetically prevent them from diffusing on to find the more stable defect sites at 300 K. Just as with the terrace sites adjacent to occupied step sites discussed above, the sites would *not* trap diffusing Ca atoms. Thus, either type of terrace site (adjacent to occupied step sites or occupied F^+ sites) could serve as the weaker binding traps which prevent Li, but not Ca, from reaching the more stable defect sites.

Thus, two types of trap sites exist for Li which are not present for Ca, and these are the dominant differences between Li and Ca in the dependence of their heat curves on defect concentration. These trap sites are (1) terrace adsorption sites at the edges of preadsorbed Li clusters, which nucleated at defects, and (2) terrace adsorption sites at the edges of Li-occupied F^+ sites.

(25) Sterrer, M.; Yulikov, M.; Fischbach, E.; Heyde, M.; Rust, H. P.; Pacchioni, G.; Risse, T.; Freund, H. J. *Angew. Chem., Int. Ed. Engl.* **2006**, *45* (16), 2630–2632.
(26) Haas, G.; Menck, A.; Brune, H.; Barth, J. V.; Venables, J. A.; Kern, K. *Phys. Rev. B* **2000**, *61*, 11105–11108.
(27) Xu, L.; Henkelman, G.; Campbell, C. T.; Jonsson, H. *Surf. Sci.* **2006**, *600*, 1351–1362.
(28) Sterrer, M.; Fischbach, E.; Risse, T.; Freund, H. J. *Phys. Rev. Lett.* **2005**, *94*, 186101.
(29) Kim, Y. D.; Stultz, J.; Wei, T.; Goodman, D. W. *J. Phys. Chem. B* **2002**, *106* (27), 6827–6830.
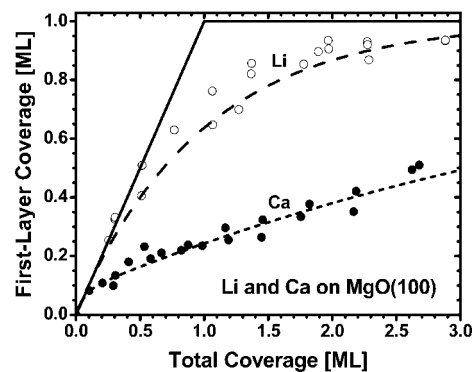(30) Carrasco, J.; Lopez, N.; Illas, F.; Freund, H.-J. *J. Chem. Phys.* **2006**, *125*, 074711.

Figure 3. Fraction of the surface covered by at least one layer versus total metal coverage for Li and Ca adsorption on pristine MgO(100) (i.e., 4−6% defects) at 300 K, as measured by ISS (points). The curves through the data represent theoretical simulations as described in the text, based on the same model as used to fit the calorimetry data in Figure 1. The solid line is the expected result for layer-by-layer growth.

The Evolution of Li and Ca Film Morphology with Coverage on MgO(100). We also used He$^+$ ion-scattering spectroscopy (ISS) to monitor the film morphology during Li and Ca deposition on unsputtered MgO(100) under conditions essentially identical to those of Figure 1. (Here we used the same time-averaged flux but it was not pulsed, so the flux was actually 20-fold less here than the peak flux during the 100-ms pulses of the calorimetry.) The results are summarized in Figure 3 and presented in more detail elsewhere for Ca[11] and Li on MgO(100).[12] Here we plot the fraction of the surface covered by at least one monolayer of the metal (i.e., the "first-layer coverage") versus the total metal coverage. Since He$^+$ ISS only gives signals for elements in the topmost atomic layer due to efficient neutralization at the low kinetic energy used here, we have taken the first-layer coverage for Ca here to be equal to the Ca ISS signal, normalized to its signal from a continuous Ca multilayer film. This assumes that the Ca signal in ISS is independent of its chemical bonding partners and is the same provided the Ca atom is in the topmost atomic layer. Since the Li ISS signal is very weak and in a low-energy region with large background in the ISS spectrum, we have taken the first-layer coverage for Li here to be equal to 1.00 minus the substrate's Mg ISS signal normalized to the Mg ISS signal from clean, Li-free MgO(100). Figure 3 shows a clear difference between Li and Ca in that the first-layer coverage of Li grows much faster with coverage than for Ca. This shows a greater tendency for Ca to pile up into 3D clusters, while Li has a greater preference for staying as 2D islands. The solid line indicates the expected growth behavior for layer-by-layer growth, which decays too quickly compared to the data for Li and especially for Ca. The solid curve through the Li data is the result expected if one assumes that intralayer Li transport is completely prohibited (i.e., no up-stepping or down-stepping between layers). Within this model, if we define y as the fraction of free sites in layer one, then the probability that an incoming Li atom land (and stay) in layer one is y. If we define θ as the total Li coverage (in monolayers), then $dy/d\theta = -y$, which integrates to give $y = \exp(-\theta)$. The fit to the data using this model is nearly within the scatter in the data and certainly far better than the layer-by-layer model, which requires facile down-stepping. This same "no up-step/no down-step model" also fit the AES data for Li/MgO(100) very well below 2 ML.[12] Note that this model is completely consistent with the site populations

predicted by the simulation model used to fit the heat curve for Li in Figure 1.

In contrast, fitting the data for Ca required a model which assumed that Ca atoms in layer one will up-step with probability 0.8 whenever they attach to the edge of an existing Ca cluster, except when bonded at a defect site. This Ca ISS model in Figure 3 was numerically propagated with tiny coverage increments using exactly the same model, computer program, and parameters as used to fit the Ca heat curve of Figure 1. That is, at each coverage increment it was assumed that each added Ca atom initially diffuses rapidly across terraces and populate defects, with this continuing until all the local defects were populated, after which each Ca atom which lands on a clean terrace site diffuses to a terrace site next to an occupied defect site, from which it up-steps with probability 0.8, or remains on a MgO site with probability 0.2. Any Ca atom which hits an occupied area on the surface was assumed to stay in layer two or higher. As can be seen, this model fits the Ca ISS data very well. These ISS results thus give support to the models used to fit the heat data.

The Li data in Figure 3 is slightly above the theoretical curve. This is probably because there is a critical 2D island size required before a new Li atom which lands on top of it will stay on top. Our model assumes it would stay even if it lands on a Li monomer. The tendency of Li to cluster into 2D islands in the first layer (see above) reduces the impact of this simplification, but it still results in a slight underestimate of the first-layer Li coverage.

The DFT results in Table 1 also explain this difference in growth morphology between Li and Ca. As shown there, a Li adatom on a MgO terrace site next to a 2D Li island is only 40 kJ/mol less stable than bulk 3D Li ($E_{ads} = 116$ vs 156 kJ/mol), and a 2D Li monolayer is almost as stable ($E_{ads} = 141$ kJ/mol). In contrast, a Ca adatom on a MgO terrace site next to a 2D Ca island is 81 kJ/mol less stable than bulk 3D Ca ($E_{ads} = 100$ vs 181 kJ/mol), and a 2D Ca monolayer is unstable compared to a bilayer. Similarly, our DFT results show that for Li, a flat pentamer is just as stable as a 3D pyramidal pentamer (within 1 kJ/mol), but for Ca this 3D pyramid is 94 kJ/mol more stable than its 2D structure. Thus, 2D Ca has a much greater thermodynamic driving force to restructure into 3D clusters than does 2D Li, and therefore up-stepping could be prohibited at 300 K for Li but not Ca.

Conclusions

The heat of adsorption has been measured for Li as a function of coverage on the surface of a MgO(100) thin film grown on Mo(100) and on MgO(100) surfaces with additional surface defects created by an Ar^+ ion beam at 300 K. The growth mode for Li was assessed by He^+ ion-scattering spectroscopy. The initial heat of adsorption is dominated by surface defects, which bind Li much more strongly than do MgO(100) terrace sites or Li clusters. Already well below a coverage of one monolayer, the heat of adsorption approaches the heat of bulk Li sublimation, due to the growth of large 2D and then 3D Li islands. Sputter damage increases the initial heat of Li adsorption and the coverage range over which it remains much higher than the heat of Li sublimation. The results are compared to previous measurements of the heats of adsorption and growth mode of

Ca on these same types of surfaces of MgO(100). The results for both metals were reasonably well fitted with a kinetic model whose essential features were determined based on DFT calculations of metal adsorption energies and adatom migration barriers (with a minor adjustment in the average adsorption energy at defects to better fit the data). The key features are

(1) Ion damage simply creates more of the same types of intrinsic defects that were present at ∼5% of the sites on the as-grown MgO(100) film.

(2) All deposited atoms are able to diffuse rapidly across MgO terraces and irreversibly bind either to an existing metal cluster or to a defect.

(3) For Ca, only defect sites are populated until all the defects are filled. After that, Ca grows exclusively on top of clusters or in terrace sites at the edges of 2D or 3D clusters (which nucleate from defects).

(4) For Li, once the defects become populated partially, it was assumed that a Li atom which lands on top of populated sites and clusters stays on top and that a Li atom which lands on free sites diffuses around and has a probability of finding an occupied defect equal to the fractional occupation of defect sites. If it finds an unoccupied defect site, it sticks there, and if it finds an occupied defect, it is trapped at the neighboring terrace site, binding to the Li atom(s) already at that defect with a heat of adsorption equal to the bulk heat of sublimation (q_{sub}).

(5) All sites on top of clusters or in terrace sites at the edges of 2D or 3D clusters were assumed to have the same heat of adsorption, equal to the heat of sublimation ($q_{sub} = 174$ kJ/mol for Ca, 159 kJ/mol for Li).

(6) The defect sites are irreversibly populated. They are mainly step and kink sites, but possibly also some more strongly binding sites.

(7) For simplicity, these defects were assumed to be present in approximately the same relative concentrations independent of the extent of ion damage (up to ∼24% defects), so that a single average defect adsorption energy (q_{defect}) could be used to fit the data (equal to 420 kJ/mol for Ca and 400 kJ/mol for Li). It is certainly expected that relaxing this simplifying assumption would allow a better fit to the data, but we did not feel it would allow better insight into the underlying phenomena beyond this simple model.

(8) Across each MgO surface there is a distribution of sizes of defect-free terrace domains, and thus a probability distribution of local defect concentrations.

This model also quantitatively reproduced the differences in growth mode for Li versus Ca, with Ca having a greater tendency to form 3D clusters at low coverage and Li growing with no interlayer migration (no up-stepping or down-stepping).